ADVANCED ENDWALL CONTOURING FOR LOSS REDUCTION AND OUTFLOW HOMOGENIZATION FOR AN OPTIMIZED COMPRESSOR CASCADE

Oliver Reutter, Magdalena Rozanski, Alexander Hergt, Eberhard Nicke

German Aerospace Center DLR, Institute of Propulsion Technology, Department Fan and Compressor, 51170 Köln, Germany, E-mail: oliver.reutter@dlr.de

ABSTRACT

The following paper deals with the development of an optimized non-axisymmetric endwall contour for reducing the total pressure loss and for homogenizing the outflow of a highly loaded compressor cascade. In contrast to former studies using a NACA-65 K48 cascade airfoil this study starts with the design of a new high performance airfoil which is based on the aerodynamic boundary conditions of the NACA-65 K48 cascade. This new airfoil is then used as a basis. Optimizations of the airfoil and of the endwall contour are performed using the DLR in-house tool AutoOpti and the RANS-solver TRACE. Three operating points at an inflow Mach number of 0.67 with different inflow angles are used to secure a wide operating range of the optimized design. The optimized endwall contour changes the secondary flow in such a way, that the corner stall is reduced, which in turn significantly reduces the total pressure loss. The endwall contour in the outflow region leads to a considerable homogenization of the outflow in the near wall region. Using non-axisymmetric endwall shaping can give a contribution to enhancing axial vane rows with already highly efficient blading.

Nomenclature

ADP	aerodynamic design point
DLR SC14-067A	DLR Subsonic Cascade designed in 2014 with $M_i = 0.67$
f1,f2	fitness functions for the endwall optimization
F1,F2	fitness functions for the airfoil optimization
H	blade height [m]
l	chord length [m]
LE	leading edge
m/M	relative mass flow [-]
m	coordinate along a streamline [m]
m′	weighted length along the streamline $m' = \int dm/r$ [-]
M_i	Mach number at inflow [-]
OP	operating point
r	coordinate in blade height direction, radius [m]
t	pitch [m]
TE	trailing edge
TGK	Transonic Cascade Test Facility at DLR Cologne
x,y,z	cartesian coordinates [m]
α	outflow angle [°]
$α_{ref}$	outflow angle of the reference [°]
$α_1$	inflow angle [°]
$α_S$	stagger angle [°]
Θ	circumferential angle coordinate [rad]
ω	total pressure loss coefficient [-]

1

Introduction

As compressors become more and more advanced, and in order to raise the efficiency and to widen the operating range, the design space has to be enlarged and three-dimensional design features have to be taken into account. Because the main flow is better understood and predicted, secondary losses have come more into focus. These losses are especially important in the rear stages of high pressure compressors, where low aspect ratios prevail. Investigations by Scholz (1954) in cascades for an aspect ratio of one show that secondary flow losses can reach up to 60 % of the total losses. Next to the possibility of three-dimensional blade shaping like sweep or lean, a good additional option for designing compressors is to use endwall contouring and shape the endwall three-dimensionally. This allows influencing secondary flow passively, thereby reducing the losses significantly. Early designs were axisymmetric like in the patents of Spear and Biedermann (1995) or of Hoeger and Schmidt-Eisenlohr (2000). Later works used non-axisymmetric attempts like in the works of Harvey (2008), Harvey and Offord (2008), Iliopoulou et al. (2008), Reising and Schiffer (2009a, 2009b), Dorfner (2009), Dorfner et al. (2011) or Heinichen et al. (2011). Overviews of endwall contouring are given in Gier et al. (2009) and Harvey (2008).

While Reutter et al. (2014) used a NACA 65 K48 airfoil as a base configuration for endwall contouring in a cascade, this study uses an optimized airfoil. It is the next step in the DLR research on endwall contouring. It is a numerical study, where as a first step an airfoil is optimized, which is then used for optimization of the endwall for a cascade setup. The endwall optimization uses optimization not only in order to reduce the losses, but also to homogenize the outflow for beneficial effects on the next stage or on the combustion chamber.

NUMERICAL SETUP

Optimization Tool AutoOpti

For the optimization the DLR in-house tool AutoOpti was used, described by Voss et al. (2006), Siller et al. (2009) and Aulich and Siller (2011). It is a multi-objective evolutionary algorithm using embedded metamodels with the expected volume gain method, described by Voss et al. (2014).

Figure 1 shows the flow chart of the optimization. The master works in the same way for both cases, airfoil or endwall design. It ranks the different geometries, called members, and stores them in a database. It uses this database together with metamodels and/or an evolutionary algorithm in order to give new promising geometries to the slaves to be calculated.

As it is very flexible the same Optimizer can be used for the airfoil optimization and the endwall optimization. Several slave-processes working in parallel are controlled by one master-process. All slaves during an optimization use the same process chain. In case of the airfoil optimization the process chain shown in the middle of Figure 1 is used by the slaves. For the airfoil optimization each slave creates an airfoil geometry by the DLR in-house tool BladeGenerator and then calculates the aerodynamic behavior for the given operating points with the 2D flow solver MISES, described by Drela and Youngren (1991), which incorporates a mesh generation.

For the endwall optimization all slaves use the process chain shown on the right hand side of Figure 1. Here a certain airfoil is used for a blade in a cascade setup with endwalls. The geometry of these endwalls is varied and a 2 mm radius fillet is added between the endwall and blade. After the mesh generation the operating points are calculated with the DLR in-house 3D-CFD-solver TRACE, for which more details can be found in Becker et al. (2010) and Franke et al. (2010). It has been validated for endwall contouring in cascade tests by Hergt et al. (2011). The transition model used is the γ-Re_Θ model implementation in TRACE described by Marciniak et al. (2014).

Of course, when optimizing a specific compressor, the blade shape and the endwall can be designed together at the same time. Here both tasks were conducted after each other in order to better separate and understand the specific effects.
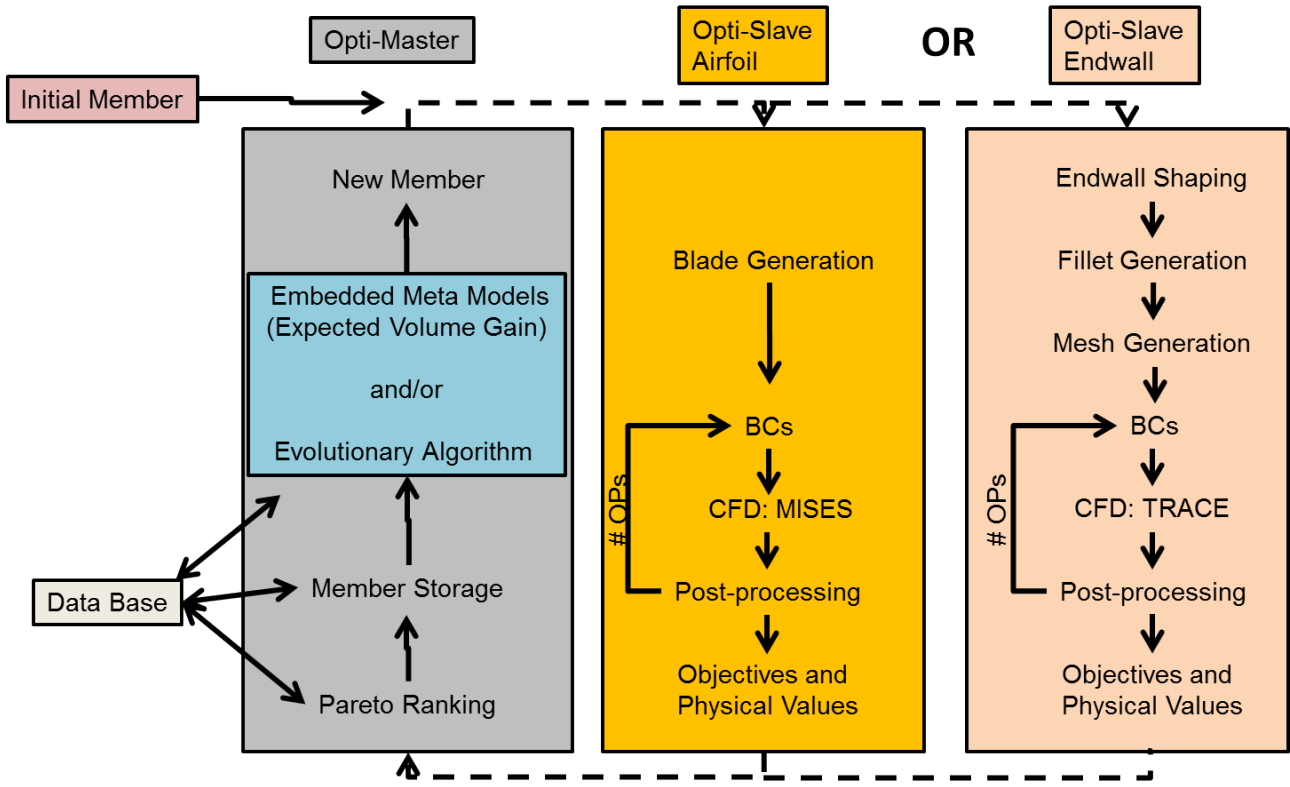
Figure 1: Flow chart of the optimization. The airfoil optimization uses the slave process chain shown in the middle; the endwall optimization uses the slave process chain on the right. The master works in the same manner for both cases.

Airfoil Optimization

In the first step a new airfoil was designed by optimization with AutoOpti. As the base geometry a NACA-65 K48 airfoil was used. Its features are described in Table 1.

Variable	NACA-65 K48 airfoil
l	70 mm
t	38.5 mm
H	168 mm
$\alpha_{1,ADP}$	42°
α_S	22.5°
M_i	0.67

Table 1: Properties of the investigated NACA-65 K48 blade cascade.

In Figure 2 the operating range of the blade cascade is shown, which has already been numerically and experimentally investigated in the Berlin DLR wind tunnel by Hergt (2011). As future experiments are now planned for the Transonic Cascade Wind Tunnel (TGK) at DLR Cologne, in contrast to the work of Hergt (2011) the profiles now have a chord length of 70 mm. In the study by Reutter et al. (2014) the numerical operating point at 44° inflow angle showed the least losses, so in this study the same operating point was chosen as the design point and called operating point 0 (OP0). The operating range, shown in Figure 2, is the operating range defined by the almost linear range of the static pressure ratio versus the inflow angle. In this operating range two further operating points are chosen for the airfoil optimization, so that the optimization does not only take the design point into account but tries to keep an operating range which is at least as large as that of the NACA airfoil. Operating point 1 (OP1) is more towards choke at an inflow angle of 38°, while operating point 2 (OP2) towards stall at an inflow angle of 51°. OP2 is the last point at which the

airfoil still raises the static pressure ratio. OP1 and OP2 angles can also be seen as the generously rounded angles, where the losses become more than double the losses in OP0 (cf. Figure 8 right hand side).
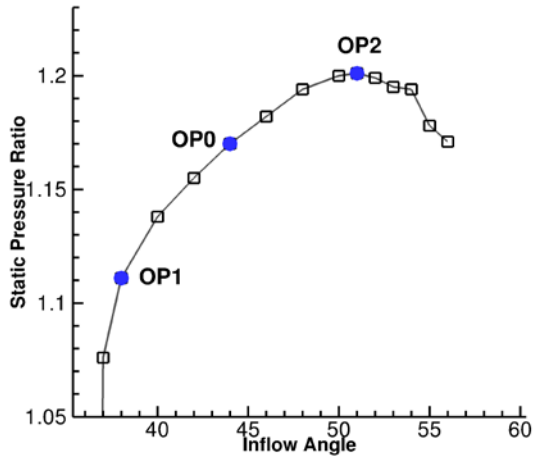
Figure 2: Static pressure ratio versus the inflow angle for the NACA airfoil.

The optimization aimed at reducing the losses in the three chosen operating points. Two objective functions were used in the optimization. As OP0 is the design point, the first fitness function aimed at reducing the losses there:

$$F1 = \omega_{OP0} \qquad (1)$$

The other fitness function was the mean value of the losses in the other operating points:

$$F2 = (\omega_{OP1} + \omega_{OP2})/2 \qquad (2)$$

Additionally, regions of interest were used, which means that certain results have to stay in a specified region. In this way the outflow angle was constricted to be in the region of 0° to 6°. This ensured an equal or larger turning than the NACA airfoil, which had an outflow angle of 6°. Also in all three operating points, the losses had to be less than the losses of the NACA airfoil in the corresponding operating point.

During the optimization 26 free parameters were used to vary the geometry. 8 parameters each were used to describe the suction and the pressure side by deBoor points. One parameter controlled the stagger angle, one the trailing and leading edge angle, four angles controlled the transition of the edges to the sides of the blade. The thicknesses of the leading and trailing edge as well as the elliptical form of the leading edge were controlled by separate parameters. More details about the airfoil parameters can be found in Lengyel et al. (2009).

The optimization was carried out on the 2D airfoil only, using the MISES flow solver. Using 2D-calculations is rather fast, so that a typical calculation takes 30 to 60 seconds on one core of a modern workstation.

Endwall Optimization

The endwall optimization was carried out similar to Reutter et al. (2014), but not using the NACA airfoil but the optimized airfoil DLR SC14-067A, the result of the optimization described above. The Operating points were the same ones as in Reutter et al. (2014), being at OP0 44°, OP1 38° and OP2 52°. So in contrast to the airfoil MISES-optimization where the OP2 is chosen at 51° for the endwall optimization the OP2 is chosen at 52° due to the larger operating range of the full cascade compared to the airfoil 2D midsection.

A constant inflow angle α_1 from the sidewall to midspan was used. Thereby the numerical results can be put in relation to the former numerical and experimental cascade investigations (Hergt 2011) and the here obtained results can be validated in future experiments in the TGK. This is in contrast to the inflow condition of a stator near the hub or shroud downstream of a rotor in real

turbomachinery applications. The inflow distribution showed a distribution in total pressure corresponding to the typical measured inlet profile of the TGK. The boundary layer on the endwall has a thickness of about 14 % of the half blade height at the inlet.

Two fitness functions were used in the endwall optimization. The first fitness function is:

$$f1 = 0.5 \cdot \omega_{OP0} + 0.25 \cdot \omega_{OP1} + 0.25 \cdot \omega_{OP2} \tag{3}$$

It is used to reduce the losses in all three operating points.

The second fitness function is an area-weighted mean of the quadratic deviation from the reference outflow angle. Here 62 cells were used for the mesh in spanwise direction:

$$f2 = \frac{r}{H}(1) \cdot [\alpha(1) - \alpha_{ref}]^2 + \sum_{62}^{k=2} \left[\frac{r}{H}(k) - \frac{r}{H}(k-1)\right] \cdot [\alpha(k) - \alpha_{ref}]^2 \tag{4}$$
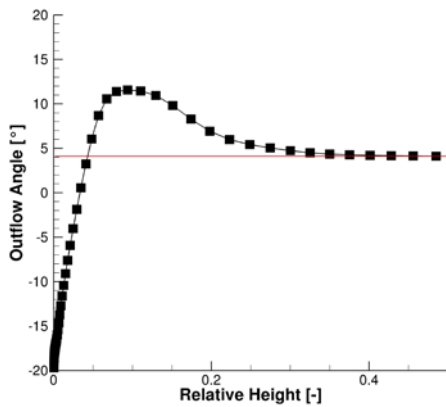
Figure 3: Outflow Angle Distribution of the DLR SC14-067A.
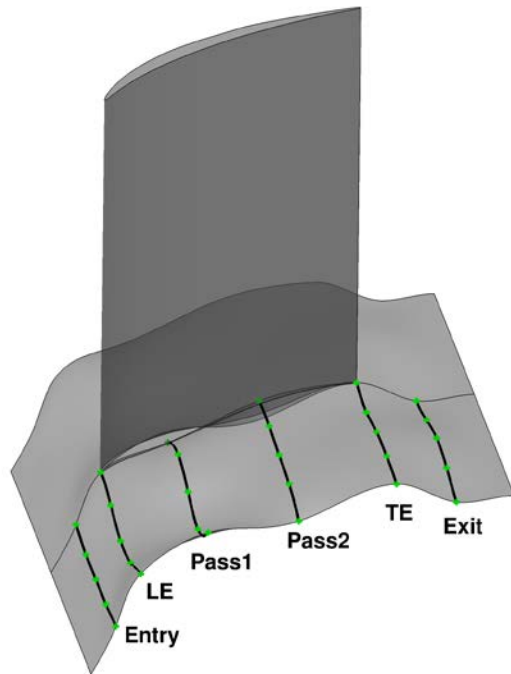
Figure 4: Endwall contouring: The six splines consisting of the control points, which define the endwall. The endwall and the blade (up to midspan) are depicted semi-transparent.

By using the quadratic angle deviation both negative and positive deviations are punished in this fitness function as well as larger deviations more than smaller ones. It is used to homogenize the outflow angle at the operating point OP0. The reference angle α_{ref} is 4.06°, which is the

5

midsection value of the outflow angle in the reference case. In Figure 3, which shows the outflow distribution of the reference cascade, it is marked by a straight red line. Near the endwall a strong overturning can be noticed, while between 4 % and 35 % span an underturning occurs. This is typical for a cascade with strong secondary flow.

The endwall is described by the same parameters as in the endwall optimization in the study of Reutter et al. (2014), 26 parameters were used to vary the endwall. The parametrization is shown in Figure 4. Each green dot is a parameter which can vary in height. At the entry, the LE, the TE and the exit the first and last points of the lines are the same to give a smooth endwall without edges. First splines are defined by these rows of points (see Figure 4), then a NURBS-surface is defined by these lines.

RESULTS

Airfoil Optimization

The airfoil optimization showed a clear Pareto front, from which a geometry was chosen. This is shown in Figure 5. It is called DLR SC14-067A.
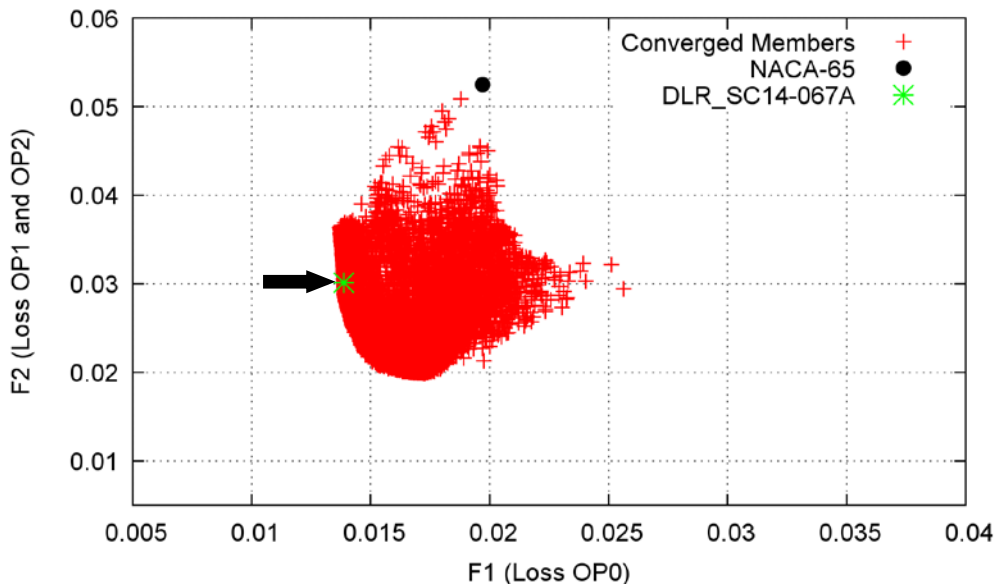
Figure 5: Pareto front of the airfoil optimization. The member DLR SC14-067A, which was chosen as the base airfoil geometry for the endwall optimization, is marked on the Pareto front.

The geometry DLR SC14-067A shows a significant improvement in the loss in OP0 and also in the combined losses in OP1 and OP2. Figure 6 shows the geometry of the base NACA airfoil and the optimized airfoil DLR SC14-067A. On the right hand side a zoom of the leading edge is shown, which shows that the leading edge is similar, the region directly after the leading edge is thicker than the NACA airfoil. Compared to the base NACA airfoil, DLR SC14-067A has a reduced stagger angle by 5°, the leading edge angle changed only by 1° and the trailing edge angle by 6°. The value of the leading edge radius became higher, but at the same time the leading edge ellipse became sharper. This parameter was also restricted, so that the ratio of the axis is no greater than 2, which is the limit against which the optimization converged. The trailing edge radius was not allowed to become smaller than 0.3 % of the chord length, which is the value against which it converged, starting from the NACA airfoil with 0.55 %.
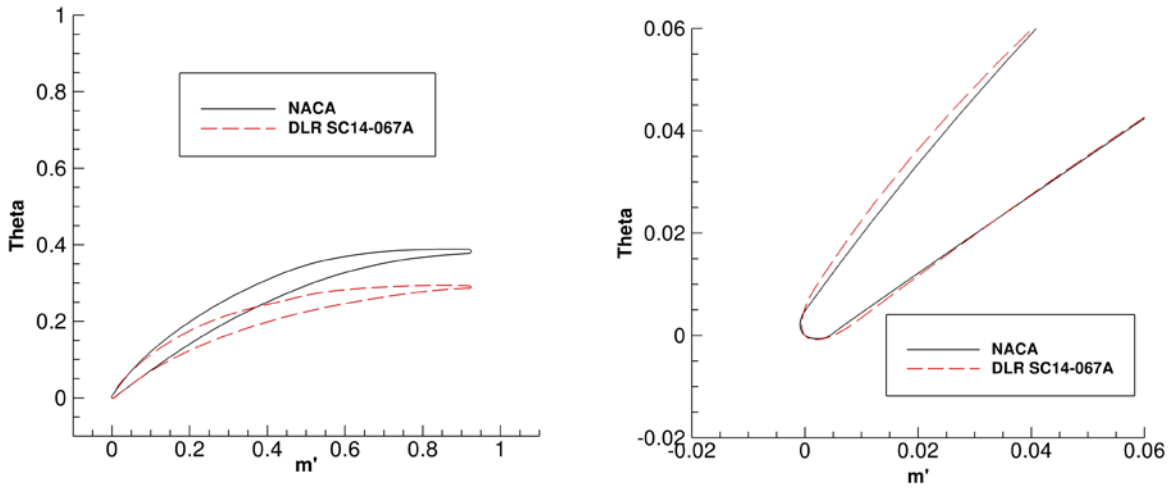
Figure 6: DLR SC14-067A (dashed red line) and NACA (black line), detail of the leading edge on the right.
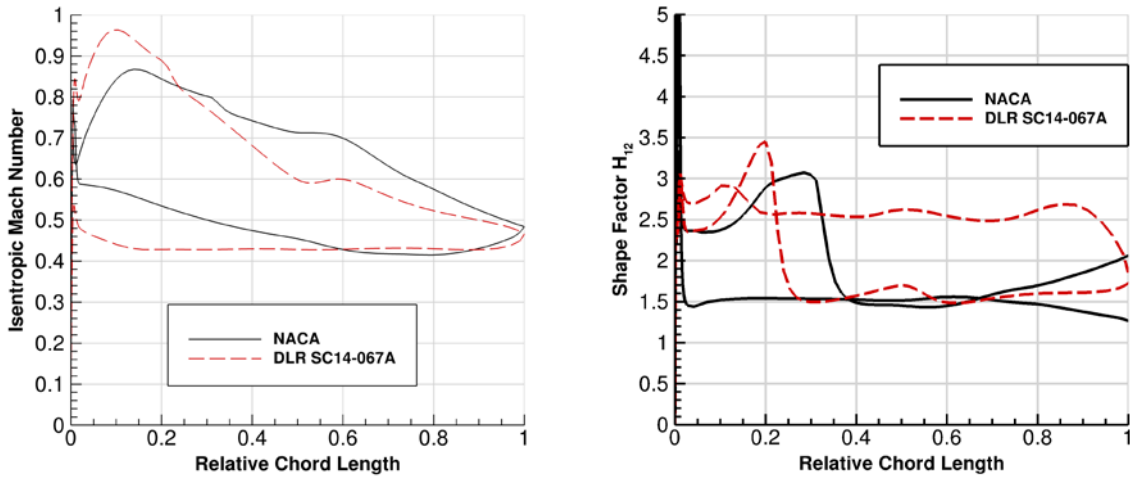
Figure 7: OP0: Isentropic Mach number distribution NACA (black line) and DLR SC14-067A (dashed red line) on the left hand side; shape factor on the right hand side.
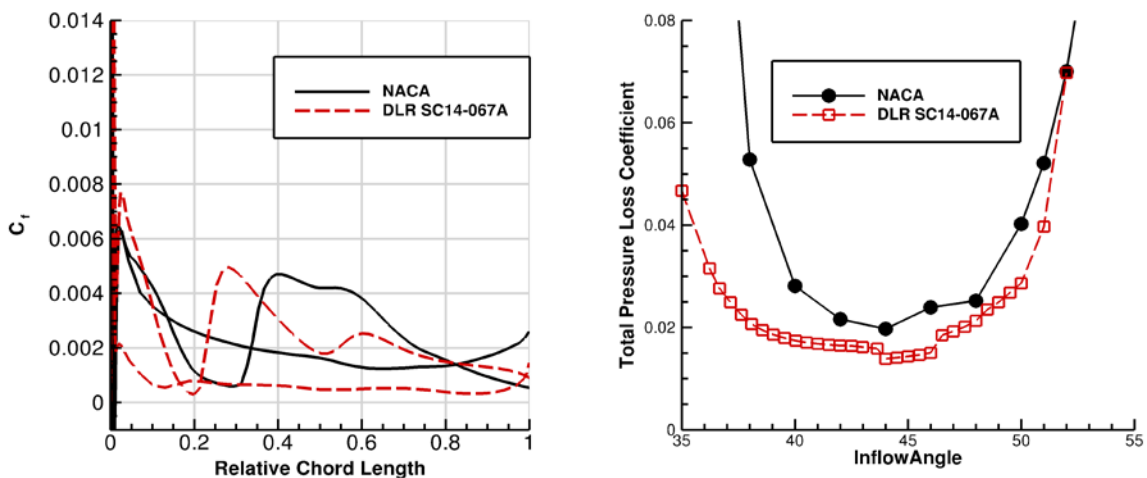
Figure 8: Friction factor for the optimized (dashed red line) and NACA (black line) airfoil on the left hand side for OP0; loss-incidence characteristics on the right hand side.

The isentropic Mach number distribution is shown in Figure 7 on the left hand side. It can be seen, that the DLR SC14-067A airfoil shows a more frontloaded design, often seen in new airfoil development projects like e.g. Siemens HPA-Airfoils, see Köller et al. (2000) and Küsters et al. (2000). It is still subsonic in OP0. On the right hand side of Figure 7 the shape factors for the two airfoils are shown. It can be seen, that the pressure side of the optimized airfoil stays laminar, where the NACA airfoil is turbulent, while on the suction side the transition of DLR SC14-067A already occurs at 20 % chord length compared to 30 % for the NACA airfoil. In Figure 8 the friction factor shows that the values are low but positive over the whole length of the airfoils. On the right hand side the loss-incidence characteristics shows that in the MISES 2D-calculations the aim of the optimization is clearly reached to design an airfoil with lower losses over the whole operating range compared to the NACA airfoil. So the DLR SC14-067A geometry was used as the base for the following endwall optimization.
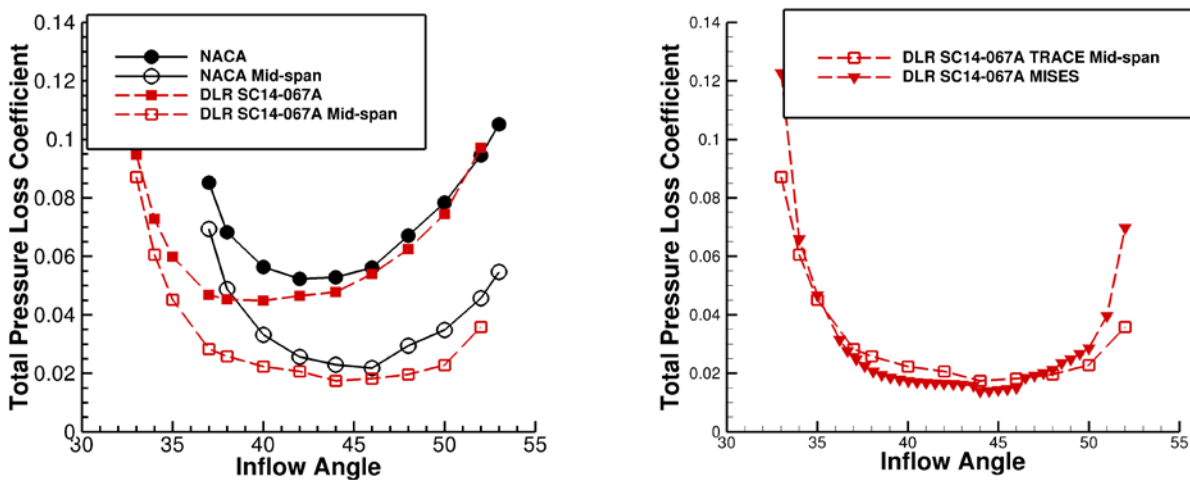
Figure 9: Inflow-angle-loss-characteristics for the calculation of the cascade setup calculated by TRACE. The results for the full cascade and only for mid-span are shown on the left hand side; the comparison of the TRACE mid-span and MISES results is shown on the right hand side.

The geometry was then studied in a cascade setup where the 3D-blades are modelled together with the smooth endwall and the constant fillet in the 3D flow solver TRACE including a transition model. The results are shown in Figure 9. One can clearly see, that the losses at midspan are close to the results of the MISES calculations (see the direct comparison for the optimized airfoil in Figure 9 right hand side), while the results for the whole cascade are much higher in losses, because of the endwall losses. The whole behavior of the DLR SC14-067A is different from the NACA cascade in the investigated angle range. The 3D-losses are close to each other at positive incidence but the lowest losses for the DLR SC14-067A occur at negative incidence in the investigated operating range and are much lower (solid symbols in Fig. 9 left).

Endwall Optimization

For the endwall optimization the blade DLR SC14-067A was used, which is the result of the airfoil optimization described above. This blade without endwall contouring, i.e. with a smooth endwall, but with a fillet around the blade was used as the reference and starting geometry for the optimization of the endwall.

Figure 10 shows the converged members of this optimization. A restriction on the resulting geometries was imposed that in the region where the underturning of the DLR SC14-067A occurs the new geometries should not have a stronger underturning in any point of the outflow angle distribution. This restriction was imposed in contrast to the study of Reutter et al. (2014), because it was found that only using the fitness function 2 was not enough to omit geometries, which showed

larger underturnings in a small region. A further restriction was that the total pressure loss coefficient had to be less than that of the base geometry with a smooth endwall in the corresponding operating point. Optimized member 555 was chosen from the Pareto frontier for further discussion.
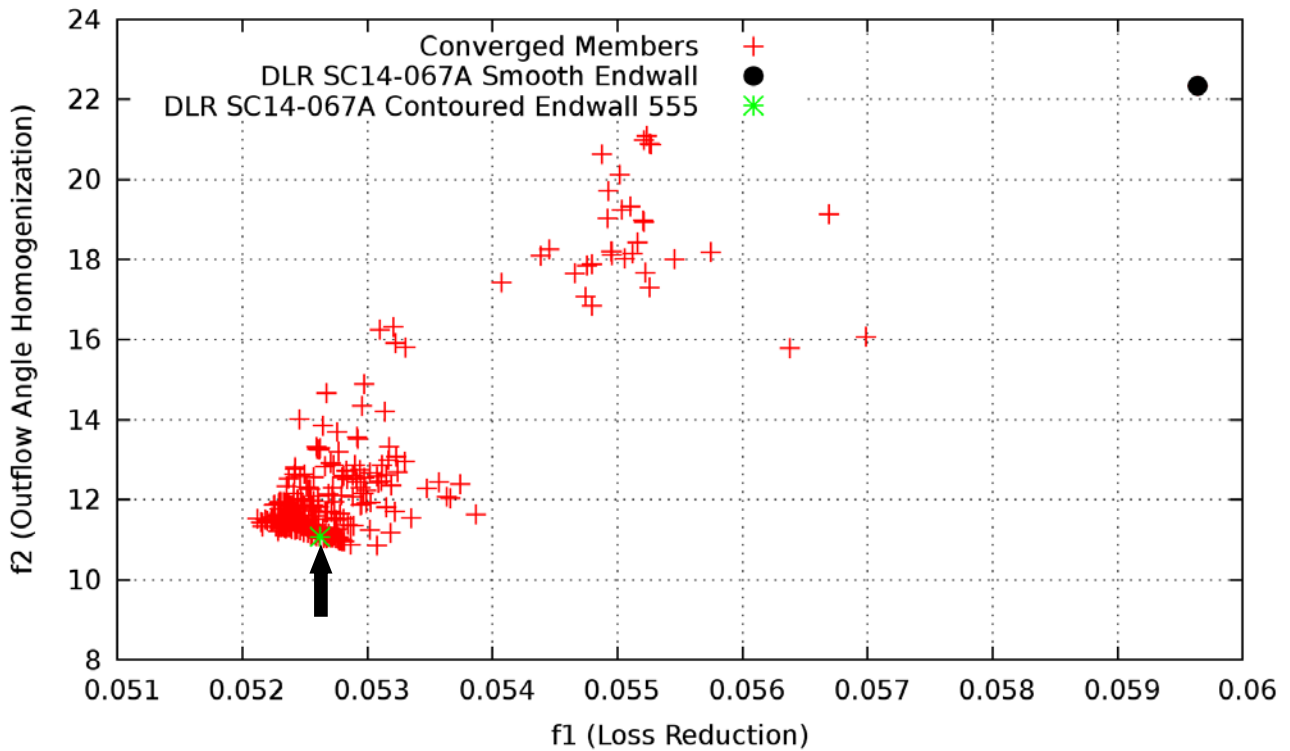
Figure 10: Geometries with the evolved Pareto front of the endwall optimization of the DLR SC14-067A cascade.

Figure 11 shows the optimized endwall member 555 as a contour plot and as a 3D-view. There is a groove along the suction side as already observed by Dorfner (2009, 2011), and a hill and valey structure behind the blade, as already observed by Reutter et al. (2014).
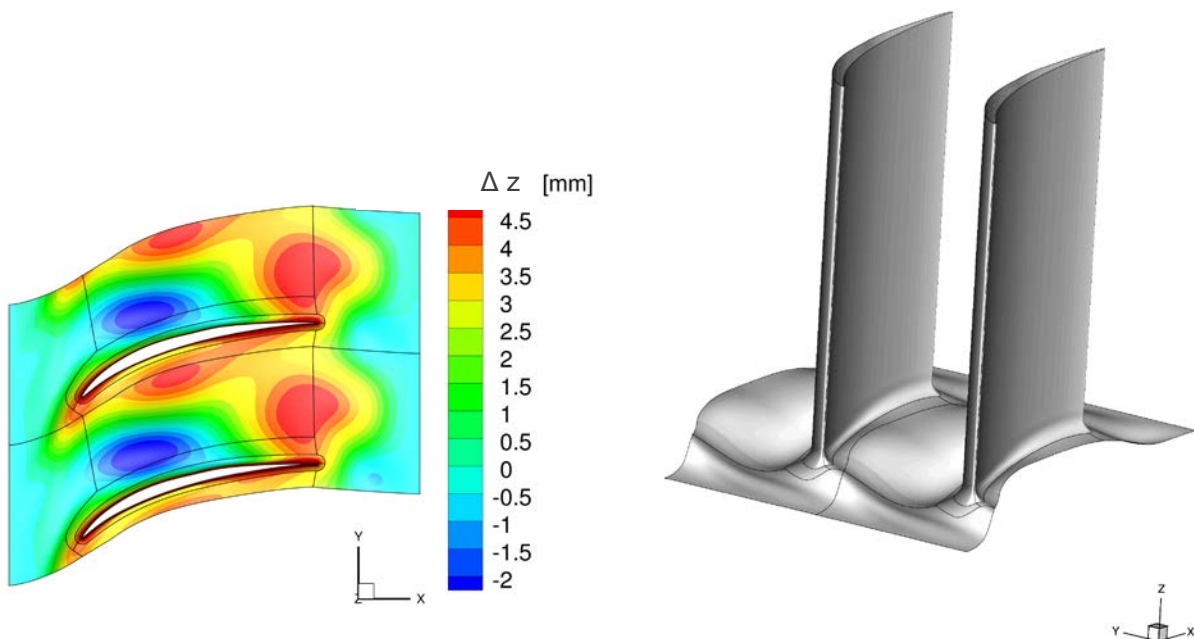
Figure 11: Height contour plot of the optimized contour member 555 on the left hand side; a 3D view looking onto the leading edge on the right hand side.

The optimization homogenized the outflow in all three operating points, see Figure 12. All graphs show the distributions over the relative mass flow m/M, and only up to 50 % relative mass flow as the calculations were conducted symmetrically. The overturning was typically reduced by 5°, the underturning by 1 °. The same effects as explained in Reutter et al. (2014) can be found here, that the corner stall is reduced and the hill and valley structure at the end of the blade helps to homogenize the outflow. But in contrast to Reutter et al. (2014), where this endwall optimization was performed using the NACA airfoil now with the DLR SC14-067A there is no loss reduction at mid-span, because the airfoil is already very good.

Looking at the total values for the losses, in fact the losses were reduced relatively for OP1 by 0.5 %, for OP0 by 9.1 % and for OP2 by 16.1 %, see Figure 13.
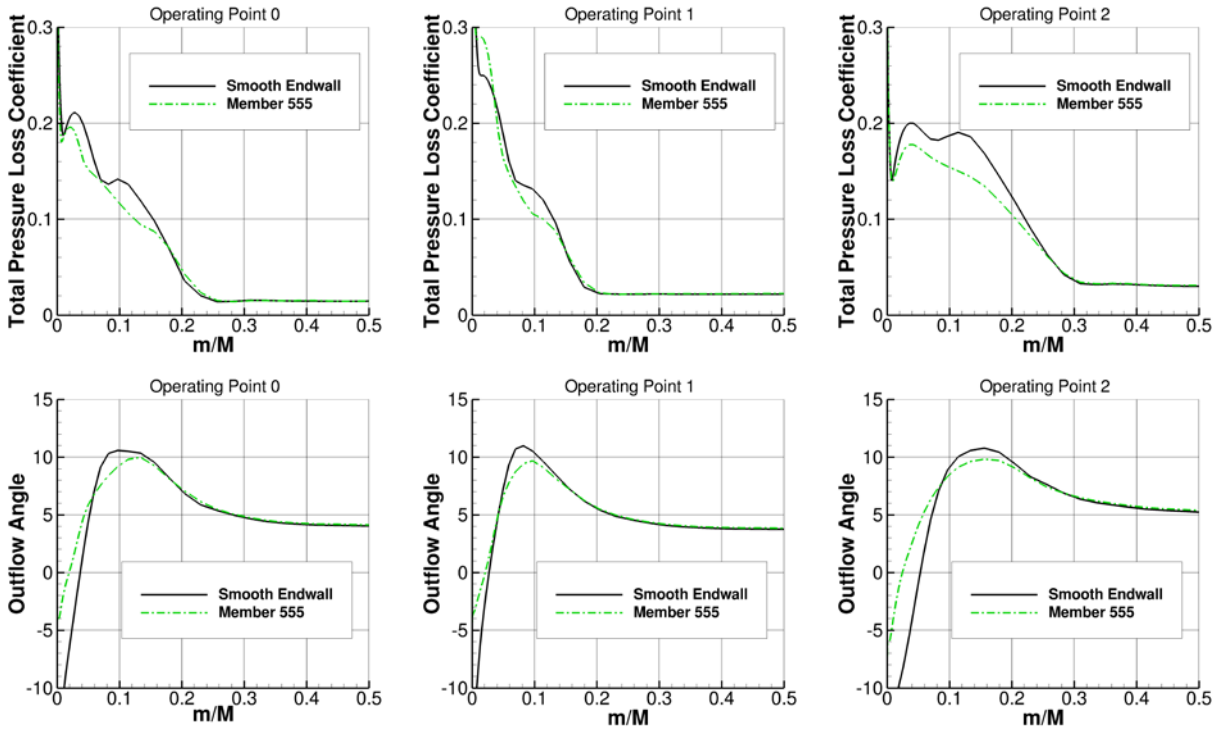
Figure 12: Loss coefficient and outflow angle for the three specified operating points.
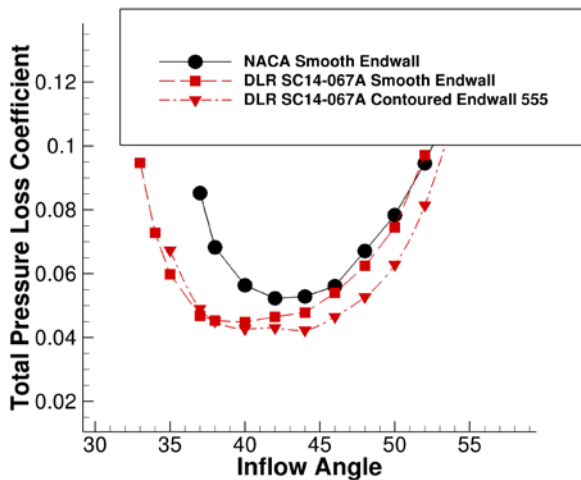
Figure 13: Loss-incidence characteristics for NACA and DLR SC14-067A cascades with smooth endwalls vs DLR SC14-067A cascade with the optimized endwall .

CONCLUSIONS

An endwall optimization was performed on the here studied DLR SC14-067A airfoil, which was specifically designed for this study to be better in turning and losses than the NACA airfoil. The results of the endwall optimization show that endwall contouring is not only an interesting option for non-optimum designs of airfoils, but also for modern designed airfoils there is an advantage in efficiency, outflow angle homogenization and widened operating range. In contrast to the endwall contouring of a NACA cascade, which has been presented in a former study, here, when using a modern designed airfoil no stronger turning and no reduced losses at midspan can be observed. Nevertheless in the region in which the endwall has influence, the lower 30 % of span, a positive effect can be seen on turning and losses. So endwall contouring is also beneficial and useful in modern designs.

For the future wind tunnel tests are planned to verify the effects observed in simulations for the optimized airfoil and endwall contouring. Furthermore based on these results a design study is planned to transfer the results into a compressor application and see e.g. how the downstream blade row can benefit from the homogenized flow angle distribution.

References

M. **Aulich** and U. Siller (2011), High-dimensional constrained multiobjective optimization of a fan stage, ASME Conference Proceedings, 2011(54679):1185–1196. doi: 10.1115/GT2011-45618.

K. **Becker**, K. Heitkamp, and E. Kuegeler (2010), Recent progress in a hybrid-grid CFD solver for turbomachinery flows, Fifth European Conference on Computational Fluid Dynamics, ECOMAS CFD 2010, Lisbon, Portugal, June 14-17

C. **Dorfner** (2009), Entwicklung eines Verfahrens zur Konstruktion nicht-rotationssymmetrischer Seitenwand-konturen in axialen Verdichtern, PhD thesis, Univer. Bochum, ISRN DLR-FB–2009-05

C. **Dorfner**, A. Hergt, E. Nicke, and R Moenig (2011), Advanced non-axisymmetric endwall contouring for axial compressors by generating an aerodynamic separator - part i: Principal cascade design and compressor application, J. Turbomach., April 2011, Vol. 133 / 021026 1- 6; DOI: 10.1115/1.4001223

M. **Drela** and H. Youngren (1991), Viscous/Inviscid method for preliminary design of transonic cascades. No. 91-2364 in AIAA-Paper.

M. **Franke**, T. Roeber, E. Kuegeler, and G. Ashcroft (2010), Turbulence treatment in steady and unsteady turbomachinery flows, Fifth European Conference on CFD, Lisbon, Portugal, June 2010.

J. **Gier**, S. Ardey, S. Eymann, U. Reinmoeller, and R. Niehuis (2002), Improving 3d flow characteristics in a multistage lp turbine by means of endwall contouring and airfoil design modification – part 2: Numerical simulation and analysis, ASMEPaper GT-2002-30353, 2002.

N. W. **Harvey** (2008), Some effects of non-axisymmetric end wall profiling on axial flow compressor aerodynamics: Part i—linear cascade investigation, ASME Conference Proceedings, 2008(43161):543–555, 2008. doi: 10.1115/GT2008-50990

N. W. **Harvey** and T. P. Offord (2008), Some effects of non-axisymmetric end wall profiling on axial flow compressor aerodynamics: Part ii—multi-stage hpc CFD study, ASME Conference Proceedings, 2008(43161):557–569, 2008. doi: 10.1115/GT2008-50991

F. **Heinichen**, V. Guemmer, A. Plas, and H.-P. Schiffer (2011), Numerical investigation of the influence of non-axisymmetric hub contouring on the performance of a shrouded axial compressor stator, CEAS Aeronautical Journal 13, December 2011, Volume 2, Issue 1-414, pp 89-98

A. **Hergt** (2011), Ueber grenzschichtbeeinflussende Maßnahmen in den Randzonen von Verdichtergittern, PhD thesis, Technical University Berlin, 2011

A. **Hergt**, C. Dorfner, W. Steinert, E. Nicke, H.-A. Schreiber (2011), Advanced nonaxisymmetric endwall contouring for axial compressors by generating an aerodynamic separator—part ii: Experimental and numerical cascade investigation, J. Turbomach. 133(2), 021027; doi: 10.1115/1.4001224

M. **Hoeger** and U. Schmidt-Eisenlohr (2000), Rotary turbomachine having a transonic compressor stage, January 25 2000. US Patent 6,017,186

V. **Iliopoulou**, I. Lepot, and P. Geuzaine (2008), Design optimization of a hp compressor rotor blade and its hub endwall, ASME Conference Proceedings, 2008(43161):2197–2208

U. **Köller**, R. Mönig, B. Küsters, H.-A. Schreiber (2000), Development of advanced compressor airfoils for heavy-duty gas turbines—part i: Design and optimization, ASME J. Turbomach., Vol. 122, No. 3, pp. 397–405

B. **Küsters**, H.-A. Schreiber, U. Köller, R. Mönig (2000), development of advanced compressor airfoils for heavy-duty gas turbines—part ii: Experimental and theoretical analysis, ASME J. Turbomach., Vol. 122, No. 3, pp. 406–414

T. **Lengyel**, T. Schmidt, C. Voß, E. Nicke (2009): Design of a counter rotating fan – an aircraft engine technology to reduce noise and CO_2-emissions, ISABE Paper, 19th ISABE Conference Montral/Canada 2009, ISABE 2009-1267

V. **Marciniak**, A. Weber, E. Kügeler (2014), Modelling transition for the design of modern axial turbomachines, 6th European Conference on Computational Fluid Dynamics, July 20 - 25 2014, Barcelona, Spain

S. **Reising** and H.P. Schiffer (2009a), Non-axisymmetric end wall profiling in transonic compressors part i: Improving the static pressure recovery at off-design conditions by sequential hub and shroud end wall profiling, ASME Turbo Expo GT2009-59133

S. **Reising** and H.P. Schiffer (2009b), Non-axisymmetric end wall profiling in transonic compressors part ii: Design study of a transonic compressor rotor using nonaxisymmetric end walls-optimization strategies and performance, ASME Turbo Expo GT2009-59134

O. **Reutter**, S. Hemmert-Pottman, A. Hergt, E. Nicke (2014), Endwall Contouring and Fillet Design for Reducing Losses and Homogenizing the Outflow of a Compressor Cascade, ASME Turbo Expo GT2014-25277

N. **Scholz** (1954), Ueber den Einfluss der Schaufelhoehe auf die Randverluste in Schaufelgittern, Forschung auf dem Gebiet des Ingenieurwesens A, 20(5):155-157,1954

U. **Siller**, C. Voss, and E. Nicke (2009). Automated multidisciplinary optimization of a transonic axial compressor, AIAA Proceedings.[np]. 05-08 Jan 2009

D.A**. Spear** and B.P. Biederman (1995), Flow directing assembly for the compression section of a rotary machine, March 14 1995. US Patent 5,397,215.

C. **Voss**, M. Aulich, B. Kaplan, and E. Nicke (2006), Automated multiobjective optimisation in axial compressor blade design, ASME Conference Proceedings, 2006(4241X):1289–1297

C. **Voss**, M. Aulich, T. Raitor (2014), Metamodel Assisted Aeromechanical Optimization of a Transonic Centrifugal Compressor, ISROMAC, 2014